The dynamics of pendant droplets on a one-dimensional surface

K. B. Glasner
Department of Mathematics, University of Arizona, 17 N. Santa Rita, Tucson, Arizona 85721, USA

(Received 8 December 2006; accepted 16 August 2007; published online 9 October 2007)

A sheet of liquid hanging from a solid surface is subject to the Rayleigh-Taylor instability, which leads to the development of pendant droplets. These near-equilibrium structures interact with the liquid film that connects them. The dynamics of the interaction can be rich and leads to large-scale patterning and nonlinear oscillations. We show that droplets move because of an energetically favorable response to asymmetries of the neighboring film thickness. The droplet moves so as to absorb the thicker liquid film and deposits a Landau-Levich film behind. In the case in which a source of fluid is introduced, the film between the droplets does not proceed toward rupture, but rather acts as a driving mechanism for migration and interaction with neighboring droplets. This interaction is shown to always be repulsive in the scaling regime investigated. A reduced system of droplet dynamics is derived asymptotically, and shows how oscillating behavior develops. © *2007 American Institute of Physics*. [DOI: 10.1063/1.2786209]

I. INTRODUCTION

It is well understood that gravity can induce instabilities in hanging liquid sheets.[1,2] Experiments[3,4] have shown that in the early phase of the instability, pendant droplets typically form a pattern that is roughly hexagonal. The early stage of this process was studied theoretically using linear and weakly nonlinear techniques[3] as well as numerically.[5] At later times, a variety of behaviors are encountered, including dripping, formation of liquid columns,[6–8] and oscillatory dynamics.[4,9] Theoretical explanations for these phenomena have been largely confined to heuristic notions from pattern formation theory,[4,6,7] and a precise connection to the fundamental fluid mechanics is still needed.

There have been relatively few theoretical investigations of pendant droplets created by the Rayleigh-Taylor instability of a thin film. Yiantsios and Higgins[10] compute numerically the evolution of a one-dimensional film toward a pattern of droplets separated by an intervening film. The subsequent drainage of this film was considered by Hammond,[11] who showed that for fixed droplets (or "lobes" in his language), the volume of fluid in the intermediate film behaves as $V \sim t^{-1/4}$. The evolution proceeds toward steady states characterized by isolated droplets separated by dry regions, which were studied by Yiantsios and Higgins[10] and Gauglitz and Radke.[12]

As with these previous works, this paper studies two-dimensional "droplets," which, precisely speaking, correspond to longitudinally uniform three-dimensional fluid ridges. (We shall use the term "droplet" here generically to describe such near-equilibrium structures.) On the other hand, many qualitative features of three-dimensional droplets moving in an effectively one-dimensional environment are reproduced, and this work is envisioned to be a point of departure to study that case. Experiments conducted by Limat *et al.*[4] consider such a setup: a fluid source is introduced on the top of a long, narrow horizontal cylinder. Droplets form on the bottom of the cylinder and evidently migrate over time.

This paper departs from previous theoretical work in two ways. First, droplets are not fixed at the boundary, but are allowed to migrate. Although this feature was noted previously,[10] it was thought to be a small effect compared to drainage of the intervening film. We also introduce a source term that constantly adds fluid in a spatially homogeneous fashion. This prevents thinning of the intervening film, which would otherwise lead to infinite-time rupture. It is therefore meaningful to study the dynamics on an intermediate timescale, where droplets are nearly at equilibrium but do not grow large enough to initiate dripping. We derive a reduced system that displays the dynamics on this timescale, whose main features are:

(1) Droplets move in a direction toward the thicker intervening film.
(2) The droplet deposits a Landau-Levitch type film as it moves, whose thickness is set by the velocity of the droplet.
(3) When neighboring droplets become close, they repel.

A large system of pendant droplets therefore comprises a chain of coupled (and highly nonlinear) oscillators.

II. GOVERNING EQUATIONS, EQUILIBRIA, AND ENERGETICS

An inertialess liquid film subject to gravity and surface tension is characterized by the Bond number $B=\rho g h_0^2/\gamma$, where ρ is the density, g the acceleration due to gravity, γ the liquid-vapor surface energy, and h_0 the mean film thickness. For small B, pendant droplets form that have small free surface slope,[10] justifying the use of the standard lubrication approximation. Since we consider the possibility of a fluid source, over time the Bond number will grow, and eventually droplets will overturn and dripping will ensue. It will be shown, however, that the rate at which the film grows is slow

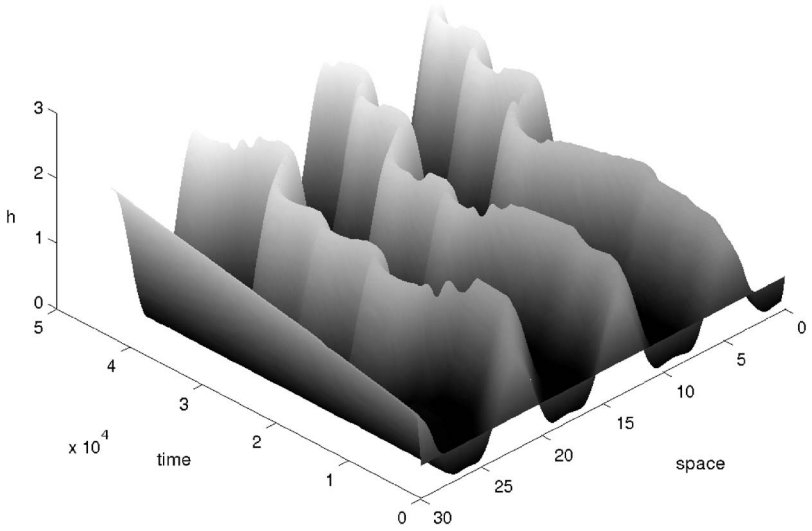

FIG. 1. Spatiotemporal plot of a numerical solution of Eq. (2).

relative to the dynamics of interest. The small-slope assumption is therefore suitable over the intermediate timescale that we consider.

The governing equations describe the evolution of a film of thickness $h(x,t)$ and pressure p, which account for the effects of gravity on a horizontal hanging film.[13,14] In nondimensional form, they are

$$h_t = (h^3 p_x)_x, \quad p = -h - h_{xx}. \tag{1}$$

Here, lengths are scaled by the capillary length $l_c = \sqrt{\gamma/\rho g}$, and time is measured with respect to the viscous timescale $3\mu/\rho g l_c$. We will also investigate the more general equation

$$h_t = F + (h^3 p_x)_x, \quad p = -h - h_{xx}. \tag{2}$$

The constant source term F accounts for a uniform addition of fluid to the system. This can be experimentally realized by condensation from the vapor[15] or transport through a porous substrate.[4] In contrast to the situation modeled by Eq. (1), the film between pendant droplets will not become arbitrarily thin at late times when $F>0$.

The boundary conditions we will use throughout the paper are reflective (Neumann) and no-flux:

$$h_x(0,t) = 0 = h_x(L,t), \quad p_x(0,t) = 0 = p_x(L,t). \tag{3}$$

These are chosen so as to isolate the phenomenon of interest and mimic conditions appropriate for a domain of infinite extent.

To illustrate the behavior that we will study, the evolution of Eq. (2) is shown in Fig. 1. The initial condition was a perturbed uniform state, and the source term was $F=10^{-5}$. After formation of quasiequilibrated droplets, migration of the droplets ensues and droplet-droplet repulsion is observed. The goal of this paper is to capture all of these features in a reduced model derived from a systematic asymptotic analysis.

A. System energy

Equation (1) has the natural energy

$$E = \int \frac{1}{2} h_x^2 - \frac{1}{2} h^2 dx, \tag{4}$$

which is the sum of surface energy and gravitational potential. The dissipation of this energy is computed to be

$$\frac{dE}{dt} = -\int h^3 ([h_{xx} + h]_x)^2 dx = -\int h^3 p_x^2 dx. \tag{5}$$

[Note that this equation follows directly from Eq. (1) by multiplying by $-(h+h_{xx})$ and integrating over the domain.] While we do not directly employ expression (5) in the later analysis, it will serve as a mechanism to simplify and interpret the analysis.

As a gradient flow, Eq. (1) cannot produce true oscillitory behavior.[10] Remarkably, we find that with the extra source term [Eq. (2)], oscillations do occur, although these are only asymptotically close to actual time-periodic solutions.

B. Equilibrium droplets

For no-flux boundary conditions, i.e., $J \equiv -h^3 p_x = 0$, equilibrium solutions of Eq. (1) are characterized as those with constant pressure and satisfy

$$-h_{xx} - h = p_0. \tag{6}$$

There is a family of positive solutions to this equation of the form [cf. Refs. 10 and 12]

$$h(x;x_0,p_0,A) = A\cos(x-x_0) - p_0, \quad A < -p_0, \quad p_0 < 0. \tag{7}$$

We will be mostly interested in isolated droplets that are surrounded by a film much thinner than the droplet's maximum thickness, given by the subclass

$$h_{\mathrm{eq}}(x;x_0,p_0) = p_0[\cos(x-x_0)+1], \quad p_0 < 0, \quad |x-x_0| < \pi. \tag{8}$$

Therefore, $h_{\mathrm{eq}}=0$ at the droplet edges: $x=x_0 \pm \pi$.

C. Energetic reason for droplet migration

Imagine a circumstance where an isolated droplet is connected to a uniform film on each side:

$$h \approx \begin{cases} \max(h_{\mathrm{eq}}, h_l), & x < x_0, \\ \max(h_{\mathrm{eq}}, h_r), & x > x_0, \end{cases} \tag{9}$$

where $h_l, h_r \ll 1$. For some translational motion, i.e., $x_0 \to x_0 + \Delta x$, fluid must be absorbed (or unabsorbed) into the droplet so that fluid volume is conserved. This amount of fluid is equal to $\Delta x(h_r - h_l)$ and is redistributed within the droplet, decreasing the gravitational potential energy. The total change in energy in both the film and the droplet can be approximated as

$$\Delta E = \Delta x\left[\tfrac{1}{2}(h_r)^2 - \tfrac{1}{2}(h_l)^2 + p_0(h_r - h_l)\right] \approx p_0(h_r - h_l)\Delta x. \tag{10}$$

Consequently, there is an energetic preference for the droplet to translate in the direction of the thicker film. The motion of the droplet can be then deduced by balancing the rate of energy change against the energy dissipation. In what follows, energy dissipation will be deduced systematically and it is shown that it occurs mostly at the droplet edges. We will also find that a Landau-Levich film is deposited at the back of the moving droplet, and therefore one may anticipate the scaling of the velocity to be $V \sim h_{l,r}^{3/2}$ (see, for example, Ref. 16).

III. MOTION OF A SINGLE DROPLET

A matched asymptotic expansion can be employed to ascertain the motion of a single droplet surrounded by a film that we take to have small characteristic thickness ϵ^2. In accord with the predicted scaling $V \sim h^{3/2}$, a timescale $T = \epsilon^3 t$ is also used.

There are three regions for the matched expansion: the droplet region, characterized as $|x - x_0(T)| < \pi$, a narrow internal layer near the droplet edges $|x - x_0(T)| = \pi$, and the thin film region $|x - x_0(T)| > \pi$. The internal layer arises to connect the discontinuous values of pressure in the droplet and thin film regions. Since we expect $h \sim h_{\mathrm{eq}}$ in the first region, h behaves quadratically near the drop edge [i.e., $h \sim -p_0(|x - x_0(T)| - \pi)^2/2$]. This motivates the introduction of a rescaled moving coordinate

$$z = [\pi - |x - x_0(t)|]/\epsilon, \tag{11}$$

which is employed to determine the internal layer solution.

A. Droplet region

In this region, the expansion $h = h_0 + \epsilon h_1 + \epsilon h_2 + \ldots$ is used. The leading order problem that determines the equilibrium solutions is

$$\{h_0^3[(h_0)_{xx} + h_0]\}_x = 0. \tag{12}$$

With the matching conditions $h_0(x - x_0 \pm \pi) = 0$ one obtains $h_0 = h_{\mathrm{eq}}(x; x_0, p_0)$, the equilibrium solutions given in Eq. (7). The next order in the expansion gives

$$\{h_0^3[(h_1)_{xx} + h_1]\}_x = 0. \tag{13}$$

Integrating and using the matching conditions $h_0(x - x_0 \pm \pi) = 0$ gives

$$(h_1)_{xx} + h_1 = C = \mathrm{const}, \tag{14}$$

whose general solution has the form

$$h_1 = A\cos(x - x_0) + B\sin(x - x_0) + C. \tag{15}$$

Equation (13) is a linear equation for h_1, which has the complementary solutions (i.e., kernel of the linear operator)

$$\Psi_1 = \sin(x - x_0), \quad \Psi_2 = \cos(x - x_0). \tag{16}$$

Fredholm solvability conditions therefore arise by taking inner product of Eq. (13) with these functions. Using Ψ_2 gives the solvability condition

$$(h_1)_x(x - x_0 - \pi) = -(h_1)_x(x - x_0 + \pi). \tag{17}$$

The next order in the expansion gives the same linear equation as for h_1:

$$\{h_0^3[(h_2)_{xx} + h_2]\}_x = 0. \tag{18}$$

A similar argument as before leads to a general solution of the form of Eq. (15). In this case, the Fredholm solvability condition uses the eigenfunction Ψ_1, leading to

$$h_2(x - x_0 - \pi) = h_2(x - x_0 + \pi). \tag{19}$$

Expressions (17) and (19) are used in conjunction with matching conditions to connect the solutions in the rescaled layer.

B. Internal layer region

The internal layer solution is expanded as $h = \epsilon^2 H(z,t) + \mathcal{O}(\epsilon^3)$, giving the leading order "traveling wave" problem

$$\sigma V H_z = (H^3 H_{zzz})_z, \tag{20}$$

where $V = dx_0/dT$ is the droplet speed. The sign σ is positive for the left-hand internal layer ($x \approx x_0 - \pi$) and negative for the right-hand one. The boundary conditions are given by matching as

$$\lim_{z\to-\infty} H = h_{l,r}, \quad \lim_{z\to-\infty} H_z = 0, \quad \lim_{z\to-\infty} H_{zz} = 0, \quad \lim_{z\to\infty} H_{zz} = -p_0. \tag{21}$$

The constants $h_{l,r}$ are the rescaled film thicknesses to the left and right of the droplet, which are derived by matching to the thin film region. In other words,

$$h(x - x_0 \pm \pi) = \epsilon^2 h_{r,l} + o(\epsilon). \tag{22}$$

Without loss of generality, it is assumed that $h_l < h_r$, so that $V > 0$ for the remainder of the discussion.

It is useful to integrate Eq. (20) once and to use the rescaled variables

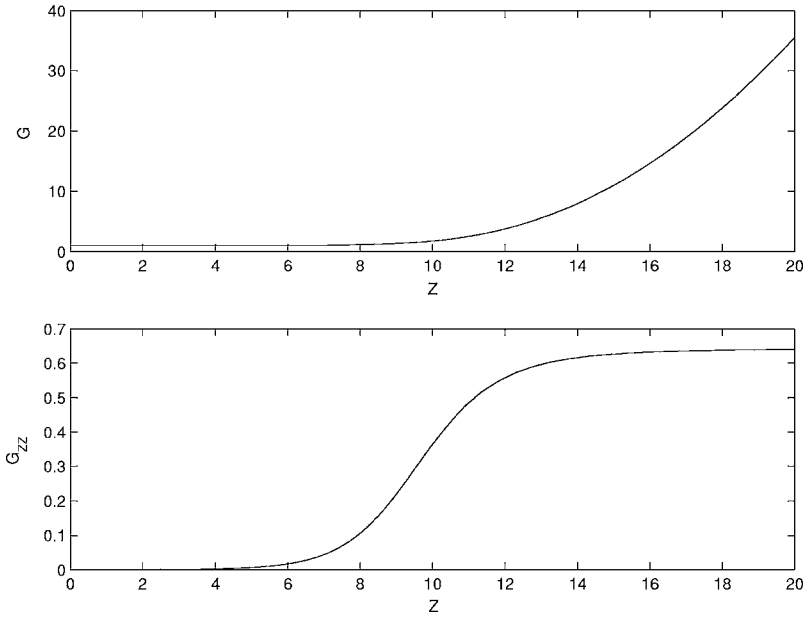

FIG. 2. Numerical solution of (24) for $\sigma=+1$.

$$G=\frac{H}{h_{l,r}}, \quad Z=\frac{V^{1/3}z}{h_{l,r}} \tag{23}$$

for each of the left- and right-hand internal layers. This leads to the third-order boundary value problem

$$\sigma(G-1)=G^3G_{ZZZ}, \quad \lim_{Z\to-\infty} G=1,$$

$$\lim_{z\to-\infty} G_Z=0, \quad \lim_{z\to\infty} G_{ZZ}=-\frac{p_0h_{l,r}}{V^{2/3}}\equiv P_{l,r}. \tag{24}$$

The left-hand layer where $\sigma=+1$ corresponds to the situation of a receding droplet. The right-hand layer has $\sigma=-1$ and corresponds to an advancing droplet. Boundary value problems of this type have been extensively explored (e.g., Refs. 17 and 18), so we summarize only the relevant features here. There is a qualitative difference between $\sigma=+1$ and $\sigma=-1$, so each is discussed separately.

The case $\sigma=+1$ corresponds to a droplet that leaves behind a uniform Landau-Levich film. A linearization around $G=1$ reveals a single unstable eigenvalue, which means that there is a unique solution (up to translation) for which $G(-\infty)\to 1$ and $G>1$. A numerical computation if this solution is shown in Fig. 2. The rescaled pressure at ∞ (basically a nonlinear eigenvalue) is computed to be

$$\lim_{z\to\infty} G_{ZZ}=P^*\approx 0.6429. \tag{25}$$

Using Eq. (24), in unscaled variables this means that

$$h_l=\frac{P^*V^{2/3}}{p_0}, \tag{26}$$

which is the anticipated Landau-Levich result (in terms of the original nondimensional scaling, the prefactor becomes the traditionally quoted value $0.643\times 3^{2/3}=1.34$).[16] It will be of interest to compute the energy dissipation of this moving structure. Multiplying Eq. (20) by H_{zz} and integrating ultimately gives

$$D_l\equiv\int_{-\infty}^{\infty} H^3H_{zzz}^2dz=\lim_{z\to\infty} H^3H_{zzz}H_{zz}-\frac{V}{2}H_z^2$$

$$=\lim_{z\to\infty} V(H-h_l)H_{zz}-\frac{V}{2}H_z^2. \tag{27}$$

This integral is finite, which can be seen by expanding the solution at infinity as

$$H\sim -p_0z^2/2+A_1z+A_0+\mathcal{O}(z^{-1}), \quad z\to\infty. \tag{28}$$

Using Eq. (27), one can compute

$$D_l=-V\left[p_0(A_0-h_l)+\frac{1}{2}A_1^2\right]. \tag{29}$$

Taking advantage of the rescaling equation (23) and using Eq. (27), this quantity can be rewritten as

$$D_l=V^{5/3}D_0=-V\left(p_0(A_0-h_l)-\frac{1}{2}A_1^2\right), \tag{30}$$

where the "dimensionless" dissipation D_0 can be evaluated numerically as

$$D_0=\int_{-\infty}^{\infty} G^3G_{ZZZ}^2dZ\approx 1.36. \tag{31}$$

The point of this computation is that Eq. (30) connects information about the internal layer solution to the matching conditions.

For the case $\sigma=-1$, linearization about $G=1$ reveals two unstable modes. There is therefore a one-parameter family of solutions corresponding to positive values of P_r (see Fig. 3), which are again unique up to translation. The energy dissipation can be computed as before, but in this case depends on the presently undetermined constant P_r. In unscaled variables, it is

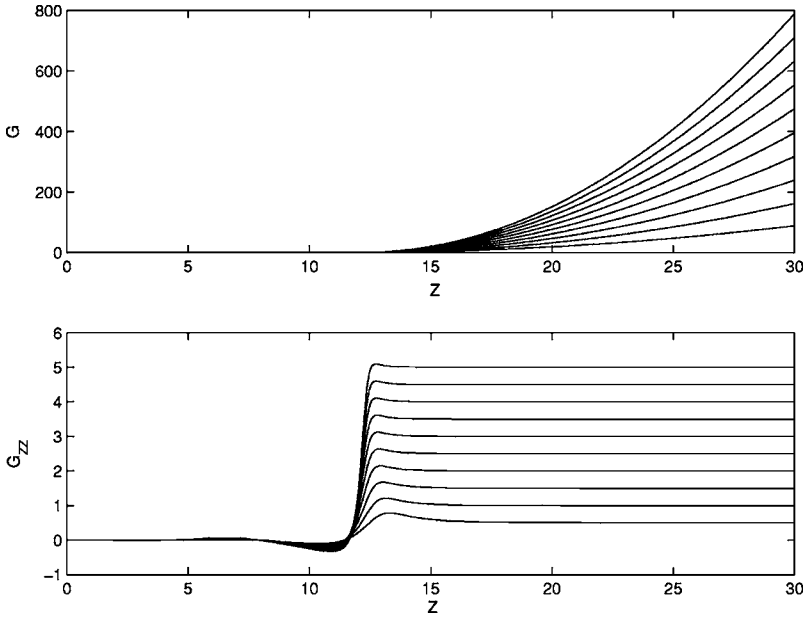

FIG. 3. Numerical solutions (24) for $\sigma=-1$. Each solution corresponds to a different value of $P_r=G_{ZZ}(+\infty)$.

$$\int_{-\infty}^{\infty} H^3 H_{zzz}^2 dz = V^{5/3} D(P_r), \quad D(P_r) \equiv \int_{-\infty}^{\infty} G^3 G_{ZZZ}^2 dZ. \tag{32}$$

Expanding

$$H \sim -p_0 z^2/2 + B_1 z + B_0 + \mathcal{O}(z^{-1}), \quad z \to \infty \tag{33}$$

and using Eq. (27) gives an expression equivalent to Eq. (29):

$$\int_{-\infty}^{\infty} H^3 H_{zzz}^2 dz = V\left(p_0(B_0 - h_r) + \frac{1}{2}B_1^2\right), \tag{34}$$

so that

$$-V\left(p_0(B_0 - h_r) - \tfrac{1}{2}B_1^2\right) = V^{5/3} D(P_r) = V^{5/3} D(-p_0 h_r / V^{2/3}). \tag{35}$$

C. Matching and dynamics

The matching conditions than connect the internal layer and droplet regions are

$$(h_1)_x(x - x_0 - \pi) = A_1, \quad (h_1)_x(x - x_0 + \pi) = -B_1,$$
$$h_2(x - x_0 - \pi) = A_0, \quad h_2(x - x_0 + \pi) = B_0, \tag{36}$$

where A_0, A_1, B_0, and B_1 are the coefficients in Eqs. (28) and (33). Adding the energy dissipation terms [Eqs. (30) and (35)] and using Eqs. (17), (19), and (36) gives

$$V p_0(h_l - h_r) = V^{5/3}[D_0 + D(-p_0 h_r / V^{2/3})]. \tag{37}$$

The motivation for this algebraic maneuver is made clear by realizing that the left-hand side represents the rate of energy change as computed heuristically in Eq. (10). Therefore, Eq. (37) is nothing more than a balance of energy and energy dissipation. Let Q be the ratio of film thicknesses. Using Eq. (26), we have

$$Q \equiv \frac{h_r}{h_l} = -\frac{h_r p_0}{V^{2/3} P^*}. \tag{38}$$

Equation (37) can then be rewritten as an equation for Q independent of any parameters

$$P^*(Q - 1) = D_0 + D(QP^*). \tag{39}$$

This equation has a unique solution that can be numerically computed, giving $Q \approx 9.8$. In other words, the ratio of advancing and receding film thicknesses must be constant (on the timescale considered), independent of the velocity or size of the intervening pendant droplet. Using Eq. (38), this gives the velocity

$$V = \left(\frac{h_r |p_0|}{QP^*}\right)^{3/2} = \left(\frac{h_l |p_0|}{QP^*}\right)^{3/2}. \tag{40}$$

Note that Eq. (40) is also the correct formula for the unscaled velocity dx_0/dt and unscaled film thickness h_l.

The previous analysis can be illustrated by a computation of Eq. (2) with $F=10^{-8}$. After a transient temporal regime, a single pendant droplet was formed, and migrated from one side of the computational domain to the other. On a logarithmic plot (Fig. 4), the internal layer structure and adjoining film thicknesses are clear. Observe that the ratio $Q=h_r/h_l \approx 10$, as predicted. Computations with different sized domains and droplets show similar results.

IV. MOTION AND INTERACTION OF MULTIPLE DROPLETS

If no fluid is added to the system ($F=0$); the thin layer between droplets will be absorbed into droplets as they migrate. This may eventually lead to film rupture, but even without rupture the timescale for the dynamics becomes longer and longer. This process can be "renormalized" by the addition of fluid, which over time will balance against the propensity of the droplets to absorb the liquid film as they

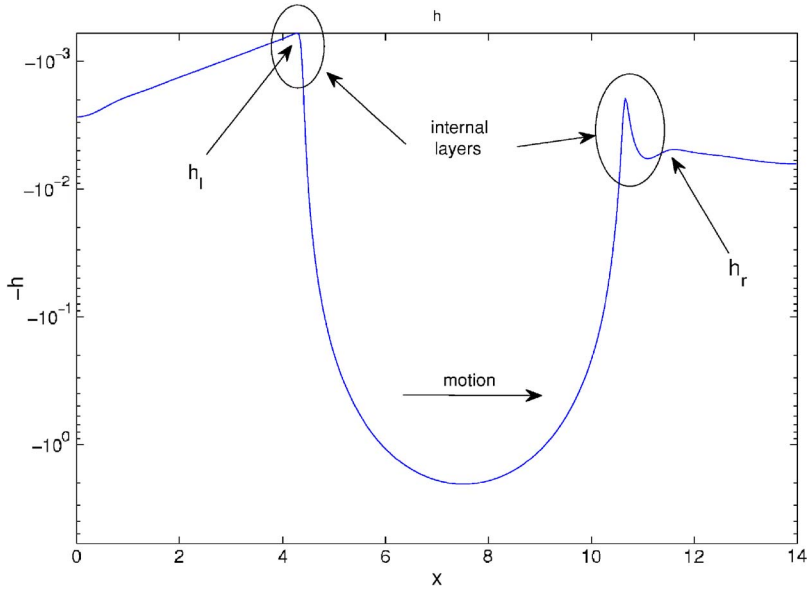

FIG. 4. (Color online) Numerical simulation of a single droplet at an intermediate timescale, showing internal layers that connect the droplet to the adjoining thin films. Note the ratio of adjoining film thicknesses is close to the predicted value of 9.8.

move. The flux of liquid absorbed into the droplets occurs at a rate proportional to the velocity times the film thickness. If the film thickness has the scale ϵ^2, the preceding calculation shows that the velocity scales like ϵ^3. This suggests that the choice of scales, i.e.,

$$F = F_0\epsilon^5, \quad T = \epsilon^3 t, \tag{41}$$

where $F_0 = \mathcal{O}(1)$, will lead to a consistent expansion. Note that the rate at which droplets grow is proportional to $F = \epsilon^5$, which is slower than the translational motion occurring on the timescale T. The growth and ultimate detachment of droplets is therefore a slower effect that will be ignored in the remainder of this work, although it could be included by systematically extending the present analysis. The separation of scales also implies that fluid does not really drain into droplets, but rather is "eaten up" as droplets move around.

A. Dynamics of the intervening film

The preceding asymptotic expansion can be amended to include the dynamics of the intervening film. The expansion in this region is $h = \epsilon^2 h_2 + \mathcal{O}(\epsilon^3)$, but the spatial variable is not rescaled. To leading order in the rescaled time variable, Eq. (2) reads

$$(h_2)_T = F_0. \tag{42}$$

In other words, to leading order the film does not flow, but rather just grows because of the source term. The initial condition for Eq. (42) depends on the history of the system. For a point x in the domain, if a droplet has migrated past x, the initial condition is just the thickness of the deposited Landau-Levich film. Conversely, if no droplet has passed through point x, then the initial conditions are just those for the partial differential equation (PDE) itself. Letting $\tau(x,t)$ be the time since the passage of a droplet at point x and time t with $\tau = t$ if no drop has passed, the solution to Eq. (42) can be written compactly as

$$h_2(x,T) = F_0\tau(x,T) + h_2[x, T - \tau(x,T)]. \tag{43}$$

B. Droplet interaction

When two droplets come into close proximity, two different outcomes might be anticipated: the motion continues and coalescence occurs, or the motion is arrested and the droplets reverse direction. Numerical observations indicate that for the regime being investigated, the droplets will reverse direction rather than merging. We will show this must be the case by considering a different combination of scaling in the asymptotic analysis.

Suppose that the distance between droplets is not $\mathcal{O}(1)$ as assumed before, but is instead comparable to the internal layer thickness $\epsilon = F^{1/5}$. With the spatial scale $z = x/\epsilon$ and film thickness $h = \mathcal{O}(\epsilon^2) = \mathcal{O}(F^{2/5})$, the only way to balance terms in Eq. (2) is to use a timescale $T' = \epsilon^2 t$, which is faster than that used for the motion of droplets. The leading order balance of terms in Eq. (2) is then

$$(h_2)_{T'} = -(h^3 h_{zzz})_z. \tag{44}$$

This is a fully dynamic equation that has the boundary conditions from matching

$$h_{zzz}(\pm\infty) \to 0, \quad h_{zz}(\pm\infty) = -p_0^{\pm}, \tag{45}$$

where p_0^+, p_0^- refer to the pressure of the droplets on the right and left, respectively.

Because we are working on a timescale faster than droplet motion, our main interest is in the late time evolution of Eqs. (44) and (45). Numerical simulations using random initial data and boundary conditions which mimic those in Eq. (45) suggest that solutions always approach a common "draining" solution, as illustrated in Fig. 5. This solution has three regions that scale differently in time. The first is the parabolic film between droplets where $h \sim t^{-1/4}$. The second is the narrow "pinch" region where $h \sim t^{-1/2}$. This region corresponds to an internal layer for pressure (Fig. 6) and utilizes a rescaled variable. The third region is that occupied by the near equilibrium droplets, and has the behavior

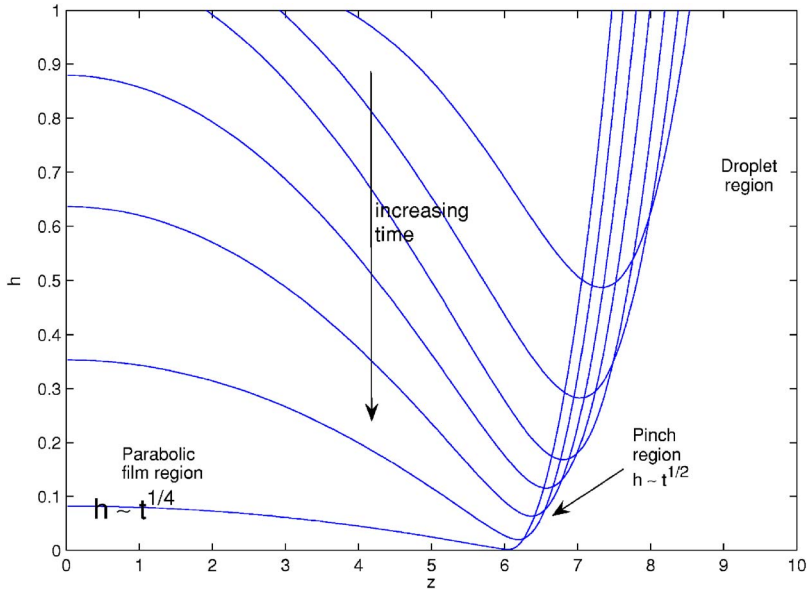

FIG. 5. (Color online) Typical numerical solution of Eq. (44), showing the approach to a common "draining" solution. The computation assumes symmetry about $z=0$. A pinch region develops near $z=6$, and the parabolic region is therefore roughly the interval $[-6,6]$.

$$h \sim -\tfrac{1}{2}p_0^{\pm}(z-z_0)^2, \tag{46}$$

where z_0 is the position of the pinch region and $p_0^{\pm}$ are the droplet pressures to the left and right. An analysis similar to the full gravitational case can be used to ascertain the solutions in each region. For simplicity, take $z=0$ to be the center of the parabolic film and $z=\pm L$ to be the location of the pinch regions.

For the parabolic film, we propose the expansion valid for large t

$$h = t^{-1/4}H_1(z) + t^{-1/2}H_2(z,t) + \cdots. \tag{47}$$

At leading order, Eq. (44) becomes

$$0 = (H_1^3(H_1)_{zzz})_z. \tag{48}$$

In other words, the parabolic film evolves quasistatically. Matching to the pinch region requires $H(\pm L)=0$, so simple integration gives the solution

$$H_1(z,t) = \frac{L\eta}{2}[1-(x/L)^2], \tag{49}$$

where the constant η is yet to be determined.

At next order in the expansion, one has the linear equation for H_2:

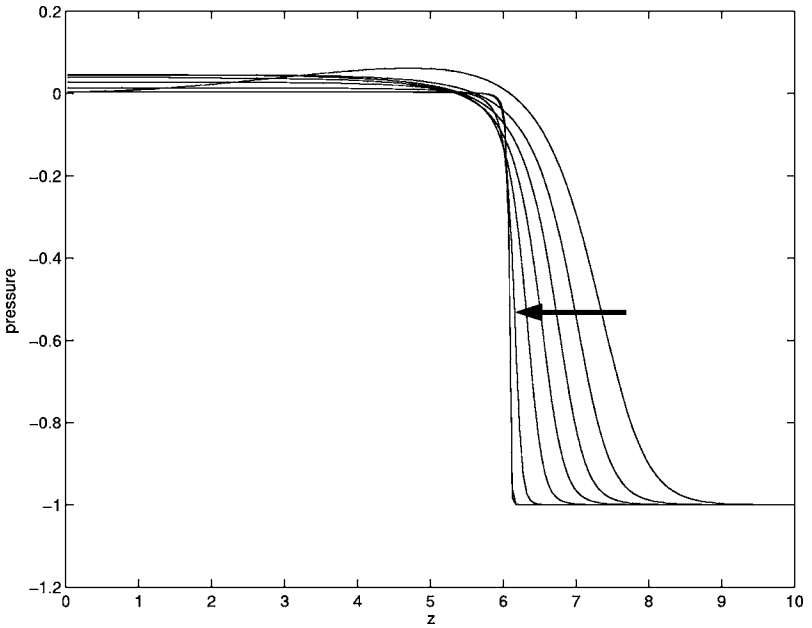

FIG. 6. Evolution of pressure, showing development and narrowing of the internal layer which is associated with the pinch region.

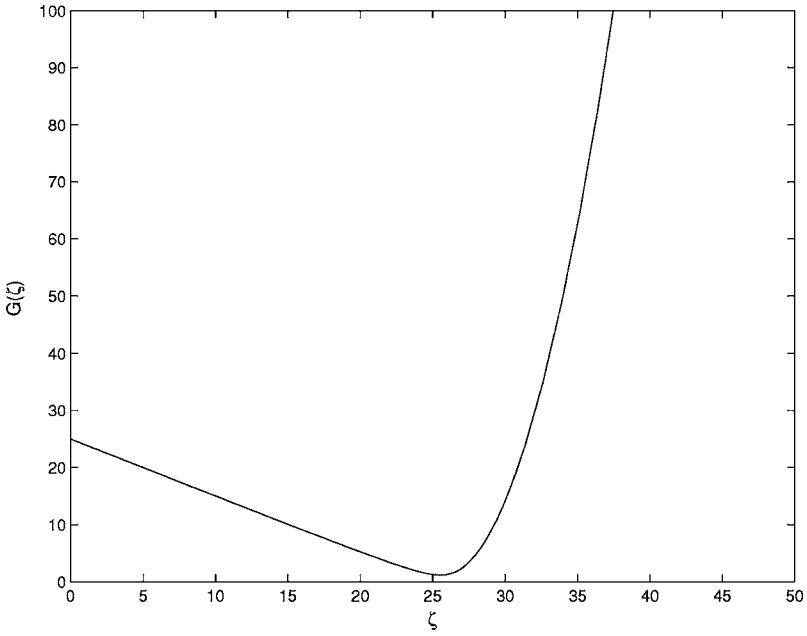

FIG. 7. Unique solution of the boundary value problem [Eq. (56)].

$$\frac{H_1(z)}{4} = [H_1^3(H_2)_{zzz}]_z. \tag{50}$$

This has a solvability condition by integrating from $-L$ to L, which gives

$$\frac{\eta L^2}{6} = J(L) - J(-L), \quad J \equiv H_1^3(H_2)_{zzz}. \tag{51}$$

For the right-hand pinch region, we use the rescaled variable $Z=(z-z_0)t^{1/4}$ and propose the expansion

$$h = t^{-1/2}H_2(Z) + o(t^{-1/2}), \tag{52}$$

again valid for large times. At leading order, this gives a steady-state equation which is the same as Eq. (44), which after one integration reads

$$H^3H_{ZZZ} = J, \tag{53}$$

where J represents the flux through this region and is yet to be determined. Matching gives the far-field boundary conditions

$$H_Z(-\infty) = -\eta, \quad H_{ZZ}(-\infty) = 0, \quad H_{ZZ}(+\infty) = -p_0^+, \tag{54}$$

where the third condition arises from Eq. (46). This problem can now be rescaled using

$$H = \frac{JG(\zeta)}{\eta^3}, \quad Z = \frac{J\zeta}{\eta^4}, \tag{55}$$

giving the third-order boundary value problem

$$G^3G''' = 1, \quad G'(-\infty) = -1, \quad G''(-\infty) = 0,$$
$$G''(+\infty) = P_2^* = -\frac{p_0^+ J}{\eta^5}. \tag{56}$$

Note that this nonlinear eigenvalue problem was also derived by Hammond,[11] who considered the drainage of an intervening film between two fixed pendant droplets.

The unique solution can be obtained numerically (see Fig. 7). In particular, we can obtain the behavior of G at $+\infty$, giving the eigenvalue $P_2^* \approx 1.22$, which means that the flux is

$$J = P_2^* D_0 \eta^5 / p_0^+. \tag{57}$$

A similar result holds for the left-hand pinch region. These expressions for J can be combined with the solvability condition (51), giving

$$\eta = \left(\frac{L^2}{6P_2^*(1/p_0^+ + 1/p_0^-)} \right)^{1/4}. \tag{58}$$

Now we return to the question of how two nearby droplets interact. In the late stage of dynamics of Eq. (44), the parabolic film becomes arbitrarily thin. Recalling that this occurs on a faster timescale than that of droplet motion, this means that the film thickness between the droplets is zero at leading order in the expansion. In light of the discussion in Sec. II C, this means that the droplets should proceed in a direction opposite of the parabolic film. In other words, droplets in close proximity will repel rather than coalesce, consistent with numerical calculations of the original equation (e.g., Fig. 1).

In considering the energetic stability of pendant droplets, Yiantsios and Higgins[10] showed that one droplet in isolation has less energy than several with the same total volume; therefore, coalescence would ultimately lower system energy. On the other hand, there is most likely an energy barrier between a two- and a one-drop configuration that prohibits coalescence. We will not elaborate further, but will leave this as a problem for further study.

V. REDUCED DYNAMICS AND OSCILLATIONS

The results of the previous two sections reduce the study of the original equation with a fluid source [Eq. (2)] to a system of ordinary differential equations coupled to a field

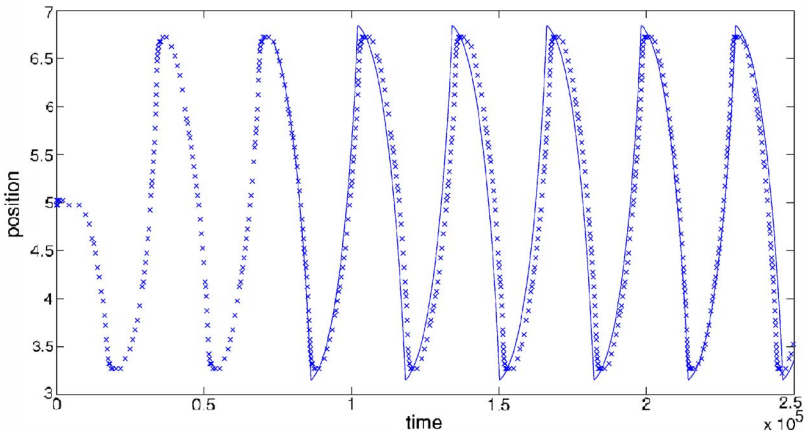

FIG. 8. (Color online) Comparison of droplet positions in the numerical solution of the PDE (x) with the reduced model (solid line). The source parameter was $F=10^{-6}$ and the spatial domain was [0,10]. Oscillations quickly approach a nearly periodic solution.

variable representing the thickness of the intervening film that evolves in a trivial fashion. Index an array of droplets from left to right so that x_i is the position of the ith drop. Restoring original scales, Eq. (40) implies that

$$\frac{dx_i}{dt} = \text{sign}[h(x_i+\pi) - h(x_i-\pi)] \times \left[\frac{\max[h(x_i-\pi), h(x_i+\pi)]|p_0|}{QP^*}\right]^{3/2}, \tag{59}$$

where the evolution of the intervening film $h(x,t)$ is given by $h_t=F$. The system is completed by the droplet repulsion condition $x_{i+1}-x_i \geqslant 2\pi$.

A. Oscillation of a single droplet

We first study the motion of just a single droplet, subject to Neumann boundary conditions. This is equivalent to reflecting symmetrically across the boundaries, so that when a droplet reaches the boundary it is repelled. A numerical simulation of the PDE based on a standard implicit finite difference method was compared to the reduced model, which is simulated as follows:

(1) The drop position(s) and intervening film thickness h are initialized using the PDE data at some specified time. The function h is represented using a uniform spatial grid.
(2) The position(s) and film thickness are each updated in time according to Eqs. (59) and (42) using a straightforward Euler method.
(3) When collisions between boundaries or other droplets are imminent, h is set to zero on a gridpoint between the droplets or the droplet and the boundary. This guarantees that the droplet(s) will reverse direction.

The PDE computation used the initial condition

$$h(x,0) = \max[\cos(x-.51)+1,\ 0.5F^{2/5}] \tag{60}$$

on the domain [0,10], which mimics the solution from the asymptotic analysis. The slight asymmetry guarantees that the droplet will migrate. Figure 8 shows the comparison between the full and reduced models for the parameter $F=10^{-6}$. The reduced model in this case used PDE data at time $t \approx 7\times 10^4$ for the initial position. Both models quickly converge to a nearly periodic solution, and both give quantitatively similar answers for the droplet trajectory. Note that in the PDE, the system volume grows and therefore exactly periodic solutions are impossible, although this effect is much slower than the period of oscillation.

B. Many-droplet system

Finally, it is interesting to observe what occurs when several droplets interact. Figure 9 shows a typical PDE numerical solution on the spatial domain [0,40]. Neumann boundary conditions pin two droplets to the boundaries, where the other ones are free to migrate. When droplets come near each other, there is a rapid draining of fluid between them, and then a reversal in direction. The net effect of these phenomenon produces a chain of coupled, nonlinear oscillators. The coupling is due both to droplet repulsion and the history of a droplets location that influences the intervening film. Figure 10 shows the position of droplets as a function of time. Although there is a characteristic period of oscillation, the motions are somewhat erratic.

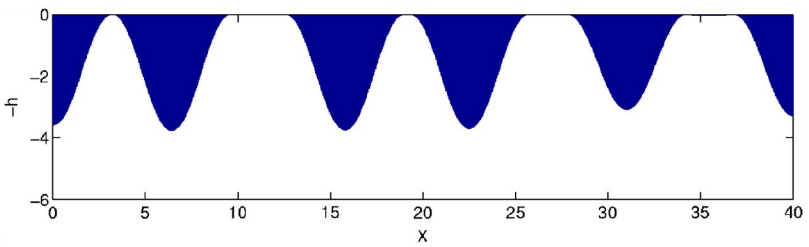

FIG. 9. (Color online) Snapshot of a typical PDE computation, showing droplets connected by a nearly indistinguishable film. The edge droplets are pinned in place because of the Neumann boundary conditions. (In this computation, $F=10^{-6}$.)

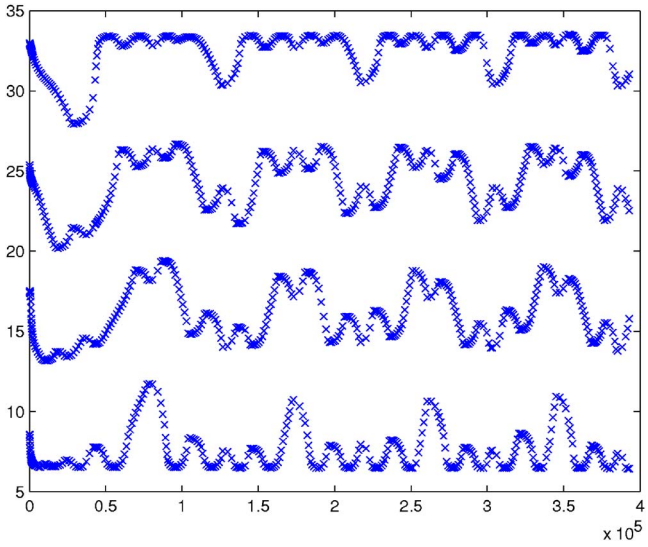

FIG. 10. (Color online) Positions of interior droplets (y axis) as in figure as a function of time (x axis), showing nonlinear oscillation ($F=10^{-6}$).

VI. DISCUSSION

It is worthwhile to comment on how our results may be generalized. Clearly, a next step is to reproduce the same arguments for the more realistic three-dimensional case. Many of features we have exploited remain intact for the three dimensional problem. In particular, a similar energetic argument can be made for migration of droplets, and the same separation of timescales for film growth and migration should hold. We also expect that droplet interaction will not necessarily involve coalescence, consistent with experimental observation.[3,4]

An important physical feature that could be included is the slope of the solid substrate, which would produce drift of droplets in the downhill direction, but would otherwise be a subdominant effect (with respect to ϵ) in the intervening thin film. Another source for substrate interaction is van der Waals forces, which should only come into play for very thin films.

In terms of broad applicability, this study belongs to a large class of dynamical situations where large scale interaction provides a mechanism for locally equilibrated structures (e.g., Ref. 19) to produce interesting collective behavior. The present results can be contrasted to the case of droplets formed from dewetting processes,[20,21] which also interact through an intervening film but whose long-time behavior is characterized by coarsening instead of dynamic patterning. The interaction of other near equilibrium structures (ridges, rivulets, liquid columns, and sheets) may also be interesting to study in a similar, reduced dimension framework.

ACKNOWLEDGMENTS

The author has benefitted from discussions with Peter Evans, Andreas Münch, and Barbara Wagner. This work was supported under NSF award DMS-0405596.

[1] Lord Rayleigh, *Scientific Papers* (Cambridge University Press, Cambridge, UK, 1900), Vol. II.
[2] G. I. Taylor, "The instability of liquid surface when accelerated in a direction perpendicular to their planes," Proc. R. Soc. London, Ser. A **201**, 192 (1950).
[3] M. Fermigier, L. Limat, J. E. Wesfreid, P. Boudinet, and C. Quillet, "Two dimensional patterns in Rayleigh-Taylor instability of a thin layer," J. Fluid Mech. **236**, 349 (1992).
[4] L. Limat, P. Jenffer, B. Dagens, E. Touron, M. Fermigier, and J. E. Wesfreid, "Gravitational instabilities of thin liquid layers: dynamics of pattern selection," Physica D **61**, 166 (1992).
[5] L. W. Schwartz, *Unsteady Simulation of Viscous Thin-Layer Flows* (Computational Mechanics Publications, Boston, 1997), pp. 203–233.
[6] C. Counillon, L. Daudet, T. Podgorski, and L. Limat, "Dynamics of a liquid column array under periodic boundary conditions," Phys. Rev. Lett. **80**, 2117 (1998).
[7] P. Brunet and L. Limat, "Defects and spatiotemporal disorder in a pattern of falling liquid columns," Phys. Rev. E **70**, 046207 (2004).
[8] P. Brunet, G. Gauthier, L. Limat, and D. Vallet, "Structure and dynamics of a bidimensional pattern of liquid columns," Exp. Fluids **37**, 645 (2004).
[9] L. Limat, F. Giorgutti, M. Fermigier, P. Jenffer, and J. E. Wesfreid, "Dynamique non-lineare d'instabilies de surface: gouttes et collones liquies formees par ruissellement de films," Rev. Gen. Therm. **36**, 672 (1997).
[10] S. G. Yiantsios and B. G. Higgins, "Rayleigh-Taylor instability in thin viscous films," Phys. Fluids A **1**, 1484 (1989).
[11] P. S. Hammond, "Nonlinear adjustment of a thin annular film of viscous fluid surrounding a thread of another within a circular cylindrical pipe," J. Fluid Mech. **137**, 363 (1983).
[12] P. A. Gauglitz and C. J. Radke, "An extended evolution equation for liquid film breakup in cylindrical capillaries," Chem. Eng. Sci. **43**, 1457 (1988).
[13] P. G. de Gennes, "Wetting: Statics and dynamics," Rev. Mod. Phys. **57**, 827 (1985).
[14] A. Oron, S. H. Davis, and S. G. Bankoff, "Long-scale evolution of thin liquid films," Rev. Mod. Phys. **69**, 931 (1997).
[15] A. Oron and S. G. Bankoff, "Dynamics of a condensing liquid film under conjoining/disjoining pressures," Phys. Fluids **13**, 1107 (2001).
[16] F. Brochard-Wyart, D. Quere, and P.-G. deGennes, *Drops, Bubbles, Pearls, Waves: The World of Capillarity* (Springer, New York, 2003).
[17] E. O. Tuck and L. W. Schwartz, "A numerical and asymptotic study of some third-order ordinary differential equations relevant to draining and coating flows," SIAM Rev. **32**, 453 (1990).
[18] B. R. Duffy and S. K. Wilson, "A third-order differential equation arising in thin-film flows and relevant to Tanner's law," Appl. Math. Lett. **10**, 63 (1997).
[19] M. J. Ward, "Dynamic metastability and singular perturbations," in *Boundaries, Interfaces, and Transitions*, edited by M. E. Delfour, CRM Proc. Lecture Notes, Banff, Alberta, Canada, 1995 (Am. Math. Soc., Providence, RI, 1998), Vol. 13, pp. 237–263.
[20] K. Glasner and T. Witelski, "Coarsening dynamics of dewetting films," Phys. Rev. E **67**, 016302 (2003).
[21] K. B. Glasner and T. P. Witelski, "Collision versus collapse of droplets in coarsening of dewetting thin films," Physica D **209**, 80 (2005).